*J. Fluid Mech.* (1984), *vol.* 147, *pp.* 233–259
*Printed in Great Britain*



# Convective flow and heat transfer in variable-porosity media

By KAMBIZ VAFAI
Department of Mechanical Engineering, The Ohio State University, Columbus

(Received 19 September 1983 and in revised form 11 May 1984)

The present work analyses the effects of variable porosity and inertial forces on convective flow and heat transfer in porous media. Specific attention is given to forced convection in packed beds in the vicinity of an impermeable boundary. After establishing the governing equations, a thorough investigation of the channelling effect and its influence on flow and heat transfer through variable-porosity media is presented. Based on some analytical considerations, a numerical scheme for the solution of the governing equations is proposed to investigate the variable-porosity effects on the velocity and temperature fields inside the porous medium. The method of matched asymptotic expansions is used to show the qualitative aspects of variable porosity in producing the channelling effect. These qualitative features are also confirmed by the numerical solution. The qualitative effects of the controlling parameters on flow and heat transfer in variable-porosity media are discussed at length. The variable-porosity effects are shown to be significant for most cases. For the same conditions as the perturbation solution, the numerical results are in excellent agreement with the perturbation analysis. The numerical results are also in very good agreement with the available experimental data of previous studies.

## 1. Introduction

The importance of porous media in a variety of different applications such as petroleum reservoirs, building thermal insulation, chemical catalytic reactors, direct-contact heat exchangers, has led to extensive investigations in this area. This increased use of porous media requires a better understanding of the associated transport processes. However, owing to the geometric complexity of the porous medium some simplifications must be introduced. Most of the existing studies, such as those by Burns & Tien (1979) and Cheng & Minkowycz (1977), deal primarily with the mathematical simplification based on Darcy's law, which neglects the effects of a solid boundary, inertial forces and variable porosity on flow through porous media. In many applications, for example packed-bed catalytic reactors, the porous medium is bounded, the fluid velocity is high (i.e. high Reynolds number based on pore diameter) and the porosity is variable; therefore it is important to investigate these boundary, inertia and variable-porosity effects. The boundary and inertia effects on convective flow and heat transfer were analysed by Vafai & Tien (1981) for constant-porosity media and expressed in terms of several governing parameters. These allowed a simple characterization scheme for interpreting the applicability of Darcy's law to various problems of flow and heat transfer in porous media. Furthermore, these effects were analysed and confirmed by an experiment (Vafai & Tien 1982) for transient mass transfer through constant-porosity media. In some

applications, such as fixed-bed catalytic reactors, packed-bed heat exchangers, drying, chemical-reaction engineering and metal processing, the constant-porosity assumption does not hold because of the influence of an impermeable boundary. Therefore there is a need to focus on the variable-porosity effects on forced convection in the vicinity of an impermeable boundary. The region close to an external boundary is of particular importance, since for most applications the quantities of interest, such as the heat flux at the boundary, are closely involved in that region.

The variable porosity close to an impermeable boundary leads to a number of important effects such as flow maldistribution and channelling. Channelling, which refers to the occurrence of a maximum velocity in a region close to an external boundary, has been reported by a number of investigators such as Schwartz & Smith (1953) and Schertz & Bischoff (1969). Their velocity measurements in packed beds show a maximum close to the boundary. Furthermore, the measurements of Roblee *et al.* (1958) and Benenati & Brosilow (1962) show a distinct porosity variation in packed beds. Their results show a high-porosity region close to the external boundary. The porosity as a function of the distance from the boundary can be obtained from these measurements. Chandrasekhara & Vortmeyer (1979) used these measurements to solve numerically for the velocity profile in isothermal packed beds. However, their result was limited, and it was not based on a general formulation of the momentum equation. Moreover, they did not investigate the heat-transfer aspects of the variable-porosity medium. Flow maldistributions in packed beds have also been considered by a number of other investigators such as Stanek & Szekely (1972).

Most of the heat-transfer investigations in packed beds, such as those of Hughmark (1976), Balakrishnan & Pei (1974), Denloye & Botterill (1977) and Schlunder (1978), are presented in terms of correlations based on Colburn–Chilton $j$-factors. These correlations express the heat transfer from the bulk of the packed bed; and the effects of the boundary and the variable porosity on the heat transfer are seldom, if ever, discussed. Furthermore, there is no detailed account of how the channelling effect is actually produced. The objective of this study is to present an in-depth investigation of the channelling effect and its influence on heat transfer and flow through variable-porosity media. First, the equations in Vafai & Tien (1981) are applied to a variable-porosity medium to derive the governing equations. Next it is shown that the velocity field is only a function of the coordinate that is normal to the boundary. The equations are then solved numerically to reveal the effects of variable porosity and inertial forces on forced convection. In addition, a singular perturbation analysis is used to explore the variable-porosity effects on the velocity field. The analysis reveals some interesting aspects of how the channelling effect is produced. Finally the qualitative effects of the controlling parameters on flow and heat transfer through variable-porosity media are demonstrated, thus enabling better predictions of heat-transfer rates in systems of this type.

## 2. Analysis

The governing equations for forced convection in porous media are developed here using the local volume-averaging technique. This is done by associating with every point in the porous medium a small volume $V$ bounded by a closed surface $A$. Let $V_f$ be that portion of $V$ containing the fluid. The local volume average of a quantity $\Phi$ associated with the fluid is then defined as in Whitaker (1969):

$$\langle \Phi \rangle = \frac{1}{V} \int_{V_f} \Phi \, \mathrm{d}V. \tag{1}$$

Using the spatial-averaging theorem, the local volume averages of the mass, momentum and energy equations for an incompressible steady flow through a variable-porosity medium are established as in Vafai & Tien (1981). The resulting equations, which assume a locally isotropic medium, are

$$\nabla\cdot\langle V\rangle = 0, \tag{2}$$

$$\frac{\mu_f}{\delta}\nabla^2\langle V\rangle - \frac{\mu_f}{K}\langle V\rangle - \frac{\rho_f F\delta}{K^{\frac{1}{2}}}[\langle V\rangle\cdot\langle V\rangle]J - \nabla\langle P\rangle^f = 0, \tag{3}$$

$$\langle V\rangle\cdot\nabla\langle T\rangle = \frac{1}{\delta}\nabla\cdot(\alpha_e\nabla\langle T\rangle), \tag{4}$$

where
$$\langle P\rangle^f = \frac{1}{V_f}\int_{V_f} P\,dV, \quad J = \frac{\langle V\rangle}{|\langle V\rangle|}, \quad \alpha_e = \frac{k_e}{\rho_f c_f}, \tag{5}$$

$\mu_f$ being the fluid viscosity, $\delta$ the porosity, $V$ the velocity vector, $K$ the permeability, $\rho_f$ the fluid density, $c_f$ the fluid heat capacity, $F$ an empirical function which depends primarily on the microstructure of the porous medium, $T$ the temperature, $J$ a unit vector oriented along the velocity vector, $\langle P\rangle^f$ the intrinsic phase average of the pressure, and $k_e$ the effective thermal conductivity of the saturated porous medium. The concept of $k_e$ has been widely used and studied (Tien & Vafai 1979). The $\mu_f\langle V\rangle/K$ term is the viscous force caused by the micropore structure. The development for momentum and the energy equations are quite different. In developing the momentum equation only the fluid phase is involved, while for the energy equation both the solid as well as the fluid phases have to be considered. The development of these equations is discussed in more detail in Vafai & Tien (1981).

### *Boundary-layer formulation for variable-porosity media*

The effects of a solid boundary on flow and heat transfer in a porous medium originate from momentum diffusion caused by the boundary frictional resistance. This resistance is in addition to the bulk frictional drag induced by the solid matrix as characterized by Darcy's law. The boundary effects are best described in terms of a new concept of a momentum boundary layer in which the above two resistances are of the same order of magnitude. This boundary-layer concept is important for the numerical solution of the governing equations.

To illustrate the important effects of variable porosity and the momentum boundary layer on flow and heat transfer, an analysis is presented for incompressible two-dimensional flow through a variable-porosity medium confined by an external boundary (figure 1). It is assumed that the porous matrix properties are all functions of the coordinate $y$. This assumption is based on using line-average (transverse to the flow) values for the porous-matrix properties. This has been shown to be a good representation for a variable-porosity medium in several experimental studies such as Roblee *et al.* (1958) and Benenati & Brosilow (1962). Furthermore, this is exactly the type of averaging that is used throughout the analysis. Therefore all the variables as well as the porous-matrix properties are line averages in the transverse direction.

Two important results are derived before obtaining the governing equations. These are $u$ = function $(y)$ and $p$ = function $(x)$ for boundary-layer flow through variable-porosity media. This is done by taking the curl of (3), invoking the boundary-layer approximations, and noting that $\delta$ and $K$ are functions of the normal coordinate $y$. This gives

$$A(y)\frac{\partial^3\langle u\rangle}{\partial y^3} + B(y)\frac{\partial\langle u\rangle}{\partial y} + C(y)\frac{\partial\langle u\rangle^2}{\partial y} + D(y)\frac{\partial^2\langle u\rangle}{\partial y^2} + E(y)\langle u\rangle + F(y)\langle u\rangle^2 = 0, \tag{6}$$

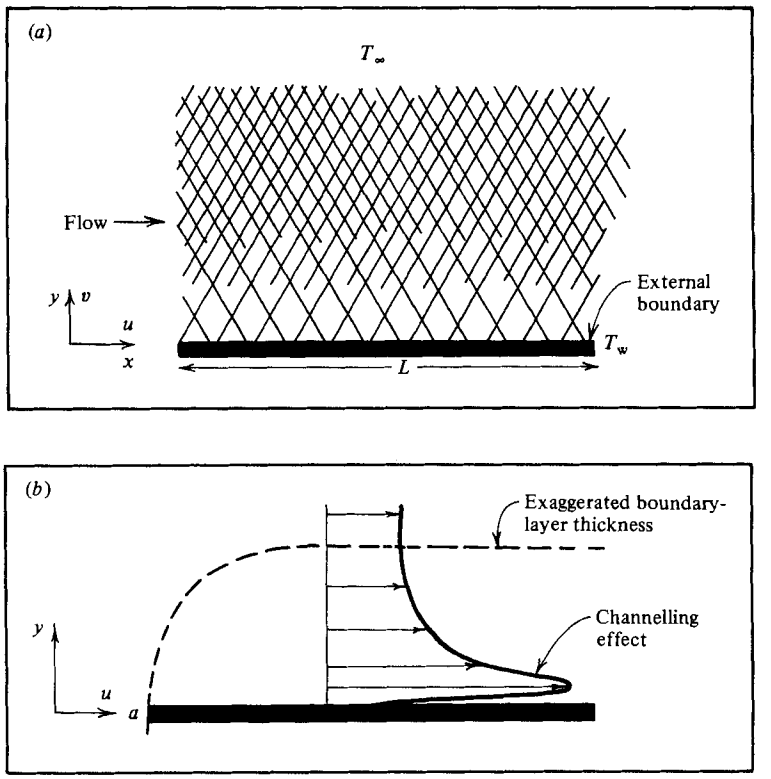


FIGURE 1. (*a*) Flow through a variable-porosity medium confined by an external boundary. (*b*) Typical velocity profile in the variable-porosity medium.

where

$$\left.\begin{aligned} A(y) &= \frac{\mu_f}{\delta}, & B(y) &= -\frac{\mu_f}{K}, & C(y) &= -\rho_f \delta^{\frac{1}{2}} F\gamma, \\ D(y) &= \mu_f \frac{\mathrm{d}\delta^{-1}}{\mathrm{d}y}, & E(y) &= -\mu_f \frac{\mathrm{d}K^{-1}}{\mathrm{d}y}, & F(y) &= -\rho_f \frac{\mathrm{d}}{\mathrm{d}y}(F\delta^{\frac{1}{2}}\gamma), \\ & & \gamma &= \left(\frac{\delta}{K}\right)^{\frac{1}{2}} \end{aligned}\right\} \tag{7}$$

For flow over an external surface the boundary conditions that go with (6) are

$$\left.\begin{aligned} \langle u\rangle &= 0 \quad \text{at} \quad y = 0, \\ \frac{\partial\langle u\rangle}{\partial y} &= 0 \quad \text{as} \quad y \to \infty, \\ \langle u\rangle &\to U_\infty \quad \text{as} \quad y \to \infty, \end{aligned}\right\} \tag{8}$$

where $U_\infty$ is the free-stream velocity. It is now clear that the solution of (6) subject to the boundary conditions given by (8) will result in

$$\langle u\rangle = \text{function of } y \text{ only.}$$

Furthermore, when there is no blowing at the surface, using the continuity and the

momentum equations it becomes apparent that

$$\langle v\rangle = 0 \tag{9}$$

and

$$\langle P\rangle^{\mathrm{f}} = \text{function of } x \text{ only.} \tag{10}$$

Therefore these results eliminate any further consideration of the continuity equation or the $y$-momentum equation. Using the above results the governing two-dimensional boundary-layer equations for forced convection through variable-porosity media are found to be

$$\frac{\mu_{\mathrm{f}}}{\delta}\frac{\mathrm{d}^2\langle u\rangle}{\mathrm{d}y^2} - \frac{\mu_{\mathrm{f}}}{K}\langle u\rangle - \rho_{\mathrm{f}} F\delta^{-\frac{1}{2}}\gamma\langle u\rangle^2 - \frac{\mathrm{d}\langle P\rangle^{\mathrm{f}}}{\mathrm{d}x} = 0, \tag{11}$$

$$\langle u\rangle\frac{\partial\langle T\rangle}{\partial x} = \frac{\alpha_{\mathrm{e}}}{\delta}\frac{\partial^2\langle T\rangle}{\partial y^2}. \tag{12}$$

It has been shown in Vafai & Tien (1981) that the boundary-layer growth is significant only over a length of the order of

$$\frac{K}{\nu}\left(-\frac{K}{\mu}\frac{\mathrm{d}\langle P\rangle^{\mathrm{f}}}{\mathrm{d}x}\right).$$

This shows that the entrance length for almost all practical cases, and certainly for packed beds, is very small and negligible.

## 3. Convection in packed beds

The governing equations developed in §2 are general and are valid for forced convection in variable-porosity media. To analyse the convection in packed beds some constitutive equations have to be supplied for the geometric function $F$ and the permeability $K$ in the momentum equation. However, the energy equation needs no modification. These constitutive equations are obtained from the experimental results of Ergun (1952). After some algebraic manipulations the constitutive equations are found to be related to the porosity and the particle diameter $d_{\mathrm{p}}$ by the following equations:

$$K = \delta^3 d_{\mathrm{p}}^2/150(1-\delta)^2, \tag{13}$$

$$F = 1.75/(\sqrt{(150)}\,\delta^{\frac{3}{2}}). \tag{14}$$

An order-of-magnitude analysis of the energy equation shows that the thermal boundary layer varies as $x^{\frac{1}{2}}$. From Vafai & Tien (1981) the momentum boundary-layer thickness is found to be of the order of $\gamma_{\mathrm{e}}^{-1}$. These results are used to transform the momentum and energy equations to achieve a very efficient and accurate numerical scheme. The transformed equations are

$$\frac{1}{\xi}\frac{\partial^2\langle\bar{u}\rangle}{\partial\eta^2} - H_1^2(\xi,\eta)\langle\bar{u}\rangle - Q(\xi,\eta)\langle\bar{u}\rangle^2 + H^2(\xi,\eta) = 0, \tag{15}$$

$$\langle\bar{u}\rangle\xi\frac{\partial\langle\theta\rangle}{\partial\xi} - \tfrac{1}{2}\langle\bar{u}\rangle\eta\frac{\partial\langle\theta\rangle}{\partial\eta} = S(\xi,\eta)\frac{\partial^2\langle\theta\rangle}{\partial\eta^2}, \tag{16}$$

where

$$\langle\bar{u}\rangle = \frac{\langle u\rangle}{u_{\mathrm{c}}}, \quad \theta = \frac{T-T_{\mathrm{w}}}{T_{\mathrm{e}}-T_{\mathrm{w}}}, \tag{17}$$

$$\eta = \frac{y\gamma_{\mathrm{e}}}{\xi^{\frac{1}{2}}}, \quad \xi = \frac{x}{L}, \tag{18}$$

$$\gamma_e = \frac{\sqrt{(150)}\,(1-\delta_e)}{\delta_e d_p}, \quad u_c = -\frac{K_e}{\mu_f}\frac{d\langle P\rangle^f}{dx}, \tag{19}$$

$$Q(\xi,\eta) = \frac{1.75[1-\delta(\xi,\eta)]\,\delta_e^2}{150(1-\delta_e)^2\,\delta(\xi,\eta)} Re_p, \quad Re_p = \frac{u_c d_p}{\nu_f}, \tag{20}$$

$$H(\xi,\eta) = \frac{\delta(\xi,\eta)}{\delta_e}, \quad H_1(\xi,\eta) = \frac{\gamma(\xi,\eta)}{\gamma_e}, \quad S(\xi,\eta) = \frac{L\alpha_e}{u_c K_e H(\xi,\eta)}. \tag{21}$$

Here $Re_p$ is the Reynolds number based on particle diameter, $T_w$ is the boundary temperature, $T_e$ the free-stream temperature, and $K_e$ and $\delta_e$ are the free-stream permeability and porosity. The corresponding boundary conditions for (15) and (16) are

$$\langle\bar{u}\rangle = 0, \quad \langle\theta\rangle = 0 \quad \text{at} \quad \eta = 0, \tag{22}$$

$$\langle\bar{u}\rangle = \frac{-1+(1+4\psi_e)^{\frac{1}{2}}}{2\psi_e}, \quad \langle\theta\rangle = 1 \quad \text{as} \quad \eta\to\infty, \tag{23}$$

where

$$\psi_e = \frac{1.75\delta_e Re_p}{150(1-\delta_e)}. \tag{24}$$

On examining the porosity variations near a wall (Benenati & Brosilow 1962) it becomes apparent that this variation is confined in a thin region close to the boundary. The wall heat flux, a convenient quantity for experimental measurements, is used to illustrate the effects of the porosity variation on heat transfer. The Nusselt number, which characterizes the wall heat flux, is expressed as:

$$Nu = \frac{-\partial\langle T\rangle}{\partial y}\bigg|_{y=0} \Big/ \frac{T_w - T_e}{L} = \frac{\gamma_e L}{\xi^{\frac{1}{2}}}\frac{\partial\langle\theta\rangle}{\partial\eta}\bigg|_{\eta=0}. \tag{25}$$

## 4. Singular perturbation analysis

The physics of the channelling effect and its production are better understood in terms of this analysis. The momentum equation (11) is solved by the method of matched asymptotic expansions. Based on the analysis in Vafai & Tien (1981), the inner-solution independent variable is chosen as

$$\bar{y} = y\left(\frac{\delta_e}{K_e}\right)^{\frac{1}{2}}, \tag{26}$$

which turns out to be a very important choice, since several other alternatives were fruitless. In the perturbation solution it is assumed that $H_1 = H$. Physically this assumption corresponds to the case where the free-stream permeability is impressed on the bulk frictional drag term throughout the porous medium. Choosing $y$ as the independent variable for the outer solution, the governing inner and outer equations are

$$\frac{d^2\langle\bar{u}\rangle}{d\bar{y}^2} - H^2(\bar{y})\langle\bar{u}\rangle - Q(\bar{y})\langle\bar{u}\rangle^2 + H^2(\bar{y}) = 0 \tag{27}$$

and

$$\frac{1}{\gamma_e^2}\frac{d^2\langle\bar{u}\rangle}{dy^2} - H^2(y)\langle\bar{u}\rangle - Q(y)\langle\bar{u}\rangle^2 + H^2(y) = 0. \tag{28}$$

The free-stream porosity $\delta_e$ is chosen as the perturbation parameter. Then a perturbation expansion of the velocity is substituted in (27) and (28). Since $H^2$ and

$Q$ are also functions of $\delta_e$, they are expanded as well. The functional dependence of the porosity on the distance from the boundary can be found from a number of experimental results such as those of Roblee *et al.* (1958) and Benenati & Brosilow (1962). These results can be represented very well by an exponential function of the form

$$\delta = \delta_e\left[1 + b\exp\left(-\frac{cy}{d_p}\right)\right]. \tag{29}$$

This result neglects the small oscillations of the porosity, which are considered to be secondary. The emphasis here is on the decay of the porosity from the external surface, which has the primary effect. The empirical constants $b$ and $c$ are dependent on the ratio of the bed to particle diameter. However, the variations of $b$ or $c$ with respect to this ratio are small. For the perturbation solution to be valid, $b$ must be less than 1. However, this turns out to be a very mild restriction, as for most applications $b$ is less than one. Since the details of the analysis are extremely lengthy, only the final results are given. The inner perturbation results in the following equations:

$$\langle\bar{u}\rangle = u_{0i} + u_{1i}\delta_e + u_{2i}\delta_e^2 + u_{3i}\delta_e^3 + u_{4i}\delta_e^4 + u_{5i}\delta_e^5 + O(\delta_e^6),$$

$$\frac{d^2u_{0i}}{d\bar{y}^2} - B_2u_{0i} + B_2 = 0, \quad u_{0i}(0) = 0; \tag{30}$$

$$\frac{d^2u_{1i}}{d\bar{y}^2} + (B_3\bar{y}u_{0i} - B_2u_{1i}) - B_3\bar{y} = 0, \quad u_{1i}(0) = 0; \tag{31}$$

$$\frac{d^2u_{2i}}{d\bar{y}^2} - (B_4\bar{y}^2 - B_3\bar{y})u_{0i} + B_3\bar{y}u_{1i} - B_2u_{2i} + (B_4\bar{y}^2 - B_3\bar{y}) = 0, \quad u_{2i}(0) = 0; \tag{32}$$

$$\begin{aligned}\frac{d^2u_{3i}}{d\bar{y}^2} &+ (B_3\bar{y} - 2B_4\bar{y}^2 + \tfrac{1}{3}B_5\bar{y}^3)u_{0i} - (B_4\bar{y}^2 - B_3\bar{y})u_{1i} \\ &+ B_3\bar{y}u_{2i} - B_2u_{3i} - B_3\bar{y} + 2B_4\bar{y}^2 - \tfrac{1}{3}B_5\bar{y}^3 = 0, \quad u_{3i}(0) = 0;\end{aligned} \tag{33}$$

$$\begin{aligned}\frac{d^2u_{4i}}{d\bar{y}^2} &+ (B_3\bar{y} - 3B_4\bar{y}^2 + B_5\bar{y}^3 - \tfrac{1}{12}B_6\bar{y}^4)u_{0i} + (B_3\bar{y} - 2B_4\bar{y}^2 + \tfrac{1}{3}B_5\bar{y}^3)u_{1i} \\ &+ (B_3\bar{y} - B_4\bar{y}^2)u_{2i} + B_3\bar{y}u_{3i} - B_2u_{4i} - B_3\bar{y} + 3B_4\bar{y}^2 \\ &- B_5\bar{y}^3 + \tfrac{1}{12}B_6\bar{y}^4 - B_8u_{0i}^2 = 0, \quad u_{4i}(0) = 0;\end{aligned} \tag{34}$$

$$\begin{aligned}\frac{d^2u_{5i}}{d\bar{y}^2} &+ (B_3\bar{y} - 4B_4\bar{y}^2 + 2B_5\bar{y}^3 - \tfrac{1}{3}B_6\bar{y}^4 + \tfrac{1}{60}B_7\bar{y}^5)u_{0i} + (B_3\bar{y} - 3B_4\bar{y}^2 \\ &+ B_5\bar{y}^3 - \tfrac{1}{12}B_6\bar{y}^4)u_{1i} + (B_3\bar{y} - 2B_4\bar{y}^2 + \tfrac{1}{3}B_5\bar{y}^3)u_{2i} + (B_3\bar{y} - B_4\bar{y}^2)u_{3i} \\ &+ B_3\bar{y}u_{4i} - B_2u_{5i} - [2B_8u_{0i}u_{1i} + (B_{10}\bar{y} - B_9)u_{0i}^2] \\ &- B_3\bar{y} + 4B_4\bar{y}^2 - 2B_5\bar{y}^3 + \tfrac{1}{3}B_6\bar{y}^4 - \tfrac{1}{60}B_7\bar{y}^5 = 0, \quad u_{5i}(0) = 0;\end{aligned} \tag{35}$$

where

$$\left.\begin{aligned} &B_2 = (1+b)^2, \quad B_3 = 2bc_1(1+b), \quad B_4 = bc_1^2(2b+1), \\ &B_5 = bc_1^3(1+4b), \quad B_6 = bc_1^4(1+8b), \quad B_7 = bc_1^5(1+16b), \\ &B_8 = \frac{\psi_1}{1+b}, \quad B_9 = \frac{(b-3)\psi_1}{1+b}, \quad B_{10} = \frac{c_1b\psi_1}{(1+b)^2}, \\ &c_1 = \frac{c}{\sqrt{150}}, \end{aligned}\right\} \tag{36}$$

and
$$\psi_1 = \frac{1.75 d_p^3}{(150)^2 \mu_f \nu_f}\left(-\frac{\mathrm{d}\langle P\rangle^f}{\mathrm{d}x}\right). \tag{37}$$

After expanding the free-stream boundary condition, the outer perturbation results:

$$\langle \bar{u}\rangle_e = u_{0e} + u_{1e}\delta_e + u_{2e}\delta_e^2 + u_{3e}\delta_e^3 + u_{4e}\delta_e^4 + u_{5e}\delta_e^5 + O(\delta_e^6); \tag{38}$$

$$\Phi^{-2}u_{0e} - \Phi^{-2} = 0, \quad u_{0e}(\infty) = 1; \tag{39}$$

$$\Phi^{-2}u_{1e} = 0, \quad u_{1e}(\infty) = 0; \tag{40}$$

$$M^2\frac{\mathrm{d}^2u_{0e}}{\mathrm{d}y^2} - \Phi^{-2}u_{2e} = 0, \quad u_{2e}(\infty) = 0; \tag{41}$$

$$M^2\left(\frac{\mathrm{d}^2u_{1e}}{\mathrm{d}y^2} + 2\frac{\mathrm{d}^2u_{0e}}{\mathrm{d}y^2}\right) - \Phi^{-2}u_{3e} = 0, \quad u_{3e}(\infty) = 0; \tag{42}$$

$$M^2\left(\frac{\mathrm{d}^2u_{2e}}{\mathrm{d}y^2} + 2\frac{\mathrm{d}^2u_{1e}}{\mathrm{d}y^2} + 3\frac{\mathrm{d}^2u_{0e}}{\mathrm{d}y^2}\right) - \Phi^{-2}u_{4e} - \psi_1\Phi u_{0e}^2 = 0, \quad u_{4e}(\infty) = -\psi_1; \tag{43}$$

$$M^2\left(\frac{\mathrm{d}^2u_{3e}}{\mathrm{d}y^2} + 2\frac{\mathrm{d}^2u_{2e}}{\mathrm{d}y^2} + 3\frac{\mathrm{d}^2u_{1e}}{\mathrm{d}y^2} + 4\frac{\mathrm{d}^2u_{0e}}{\mathrm{d}y^2}\right) - \Phi^{-2}u_{5e}$$
$$-[2\psi_1\Phi u_{0e}u_{1e} + \psi_1(4\Phi - 1)u_{0e}^2] = 0, \quad u_{5e} = -3\psi_1; \tag{44}$$

where
$$M = \frac{d_p}{\sqrt{150}}, \quad \Phi = [1 + b\exp(-py)]^2, \quad p = \frac{c}{d_p}. \tag{45}$$

In examining these equations it becomes clear that the effects of the inertial forces is introduced at the $\delta_e^4$ term and beyond. This effect is felt simultaneously in both the governing equations and the boundary conditions. Furthermore, it is shown that these terms are necessary for the production of the so-called channelling effect. The solutions of these equations are

$$u_{0i} = 1 - \exp(-B_2^1\bar{y}), \tag{46}$$

$$u_{1i} = \alpha_4\bar{y}^2\exp(-B_2^1\bar{y}) + \alpha_1\bar{y}\exp(-B_2^1 y), \tag{47}$$

$$u_{2i} = Z_1\bar{y}^4\exp(-B_2^1\bar{y}) + Z_2\bar{y}^3\exp(-B_2^1\bar{y}) + Z_3\bar{y}^2\exp(-B_2^1\bar{y}) + Z_4\bar{y}\exp(-B_2^1 y), \tag{48}$$

$$u_{3i} = X_1\bar{y}^6\exp(-B_2^1\bar{y}) + X_2\bar{y}^5\exp(-B_2^1\bar{y}) + X_3\bar{y}^4\exp(-B_2^1\bar{y}) + X_4\bar{y}^3\exp(-B_2^1\bar{y}) + X_5\bar{y}^2\exp(-B_2^1\bar{y}) + X_6\bar{y}\exp(-B_2^1\bar{y}), \tag{49}$$

$$u_{4i} = A\exp(-B_2^1\bar{y}) + Y_1\bar{y}^8\exp(-B_2^1\bar{y}) + Y_2\bar{y}^7\exp(-B_2^1\bar{y}) + Y_3\bar{y}^6\exp(-B_2^1\bar{y}) + Y_4y^5\exp(-B_2^1\bar{y}) + Y_5\bar{y}^4\exp(-B_2^1\bar{y}) + Y_6\bar{y}^3\exp(-B_2^1\bar{y}) + Y_7\bar{y}^2\exp(-B_2^1\bar{y}) + Y_8\bar{y}\exp(-B_2^1\bar{y}) + Y_{11}\exp(-2B_2^1\bar{y}) + Y_{12}, \tag{50}$$

$$u_{5i} = F\exp(-B_2^1\bar{y}) + R_1\bar{y}^{10}\exp(-B_2^1\bar{y}) + R_2\bar{y}^9\exp(-B_2^1\bar{y}) + R_3\bar{y}^8\exp(-B_2^1\bar{y}) + R_4\bar{y}^7\exp(-B_2^1\bar{y}) + R_5\bar{y}^6\exp(-B_2^1\bar{y}) + R_6\bar{y}^5\exp(-B_2^1\bar{y}) + R_7\bar{y}^4\exp(-B_2^1\bar{y}) + R_8\bar{y}^3\exp(-B_2^1\bar{y}) + R_9\bar{y}^2\exp(-B_2^1\bar{y}) + R_{10}\bar{y}\exp(-B_2^1\bar{y}) + R_{12}\bar{y}^2\exp(-2B_2^1\bar{y}) + R_{13}\bar{y}\exp(-2B_2^1\bar{y}) + R_{14}\exp(-2B_2^1\bar{y}) + R_{15}\bar{y} + R_{16}, \tag{51}$$

$$u_{0e} = 1, \quad u_{1e} = 0, \quad u_{2e} = 0, \quad u_{3e} = 0, \tag{52}$$

$$u_{4e} = -\psi_1[1 + b\exp(-py)]^{-3}, \tag{53}$$

$$u_{5e} = -\psi_1\{4[1 + b\exp(-py)]^{-3} - [1 + b\exp(-py)]^{-2}\}. \tag{54}$$

The coefficients for these equations are given in the Appendix. On examining the governing equations for the outer perturbation it becomes clear that the outer boundary conditions are satisfied automatically. Moreover, comparing the inner and outer solutions it can be seen that, for the case where $H_1 = H$, the inertial forces are necessary for producing the constants $Y_{12}$ and $R_{16}$. These constants are in turn needed to produce the channelling effect. These constants and the changes in the free-stream boundary condition become important for terms involving $\delta_e^4$ and higher powers. Finally, in matching the inner and outer solutions, $y_\Delta[O(1)]$ is chosen as the common variable. Expressing the inner and outer variables in terms of $y_\Delta$ will result in

$$y = \Delta y_\Delta, \tag{55}$$

$$\bar{y} = \gamma_e \Delta y_\Delta, \tag{56}$$

where

$$\frac{1}{\gamma_e} \ll \Delta \ll 1,$$

so that

$$\Delta\gamma_e \gg 1. \tag{57}$$

The perturbation parameter $\delta_e$ must also be expressed in terms of $\gamma_e$. This is done by using (19), which results in

$$\delta_e = \frac{G}{\gamma_e}\left[1 - \frac{G}{\gamma_e} + \frac{G^2}{\gamma_e^2} - \frac{G^3}{\gamma_e^3} + \frac{G^4}{\gamma_e^4} \cdots\right], \tag{58}$$

where

$$G = \frac{\sqrt{150}}{d_p}. \tag{59}$$

After casting the inner and outer variables in terms of $y_\Delta$, then in the limit of

$$\Delta \to 0, \quad \gamma_e \to \infty \tag{60}$$

both the inner and outer solutions approach the same limiting value given by

$$\lim_{\substack{\Delta\to 0 \\ \gamma_e\to\infty}} \langle\bar{u}\rangle_i = \lim_{\substack{\Delta\to 0 \\ \gamma_e\to\infty}} \langle\bar{u}\rangle_e = 1 - \psi_1\left[\frac{G^4}{(1+b)^3} + \frac{3bc_1\Delta y_\Delta}{(1+b)^4}G^5\right]\frac{1}{\gamma_e^4}. \tag{61}$$

Therefore the matching of the inner and the outer solutions is done automatically. This was expected, since there were no unknown coefficients in the inner and outer solutions. For the same conditions as the perturbation solution, the perturbation and the numerical results are in excellent agreement with the perturbation solution. The plots of these solutions are given in §5.

## 5. Results and discussion

In analysing the effects of variable porosity on forced convection, (15) and (16) should be solved numerically. All of the coefficients in (15) and (16) are functions of $\xi$ and $\eta$. This is because $Q$, $H$ and $S$ are functions of the porosity and the permeability, which are in turn functions of $\xi$ and $\eta$. The functional relation between the permeability and porosity is given in (13).

| Figures | Fluid | Pressure gradient (N m$^{-3}$) | $u_c$ (m s$^{-1}$) | $d_p$ (m) | $\delta_e$ | $b$ | $c$ | $Re_p$ | Condition |
|---|---|---|---|---|---|---|---|---|---|
| 2–5 | water | 1493 | 0.325 | 0.008 | 0.5 | 0.98 | 2 | 2645 | — |
| 6–8 | water | 746 | 0.162 | 0.008 | 0.5 | 0.98 | 2 | 1322 | L |
| 6–8 | water | 1493 | 0.325 | 0.008 | 0.5 | 0.98 | 2 | 2645 | M |
| 6–8 | water | 2985 | 0.65 | 0.008 | 0.5 | 0.98 | 2 | 5290 | H |
| 9–11 | water | 1493 | 0.0812 | 0.004 | 0.5 | 0.98 | 2 | 331 | L |
| 9–11 | water | 1493 | 0.325 | 0.008 | 0.5 | 0.98 | 2 | 2645 | M |
| 9–11 | water | 1493 | 1.30 | 0.016 | 0.5 | 0.98 | 2 | 21160 | H |
| 12–14 | water | 1493 | 0.116 | 0.008 | 0.4 | 0.98 | 2 | 940 | L |
| 12–14 | water | 1493 | 0.196 | 0.008 | 0.45 | 0.98 | 2 | 1593 | M |
| 12–14 | water | 1493 | 0.325 | 0.008 | 0.5 | 0.98 | 2 | 2645 | H |
| 15–17 | water | 1493 | 0.325 | 0.008 | 0.5 | 0.6 | 2 | 2645 | L;*b* |
| 15–17 | water | 1493 | 0.325 | 0.008 | 0.5 | 0.98 | 1 | 2645 | L;*c* |
| 15–17 | water | 1493 | 0.325 | 0.008 | 0.5 | 0.98 | 2 | 2645 | M;*c* |
| 15–17 | water | 1493 | 0.325 | 0.008 | 0.5 | 0.98 | 5 | 2645 | H;*c* |
| 18 | engine oil | 1493 | 0.0003 | 0.008 | 0.5 | 0.98 | 2 | 0.0023 | L |
| 18 | engine oil | $1.2 \times 10^5$ | 0.0266 | 0.008 | 0.5 | 0.98 | 2 | 0.189 | M1 |
| 18 | engine oil | $9.9 \times 10^5$ | 0.213 | 0.008 | 0.5 | 0.98 | 2 | 1.51 | M2 |
| 18 | engine oil | $1.2 \times 10^7$ | 2.66 | 0.008 | 0.5 | 0.98 | 2 | 18.9 | H |
| 18–19 | engine oil | $1.2 \times 10^5$ | 0.0266 | 0.008 | 0.5 | 0.98 | 2 | 0.189 | M1 |

TABLE 1. Physical data for figures 2–19. L, M and H are respectively assigned to the lowest, the middle and the highest values of the physical parameter under consideration.

The numerical scheme is based on finite-difference versions of (15) and (16), supplied with the boundary conditions given in (22) and (23). The upstream condition for the energy equation is taken as uniform temperature $T_\infty$ at $x = 0$. The finite-difference scheme was based on using upwind differencing in the $\xi$-direction, and an implicit routine in the $\eta$-direction, along with the linearization of the momentum equation. The resulting set of algebraic equations was solved by tridiagonalizing the solution matrix. The linearization scheme used for (15) was checked by increasing the number of iterations used for convergence. The numerical scheme resulted in a very efficient and stable system. The accuracy of the finite-difference solution was tested by increasing the number of gridpoints, and investigating some limiting cases.

In obtaining the numerical results the following input parameters were used: the driving pressure force, the particle diameter $d_p$, the free-stream porosity $\delta_e$, the empirical constants $b$ and $c$ in (29), and the thermophysical properties of the fluid and the solid matrix. The free-stream permeability and the effective thermal conductivity were calculated from these input data. The free-stream permeability was found from (13). This equation was checked against the semiempirical formulation recommended in DeWiest (1969), which also relates the permeability to porosity and the particle diameter. The agreement was found to be good. The effective thermal conductivity was found in terms of a statistical upper and lower bound given in Tien & Vafai (1979) as

$$F_1(\delta, R, G) \geqslant \frac{k_e}{(k_s k_f)^{\frac{1}{2}}} \geqslant F_2(\delta, R, G). \tag{62}$$

Here $k_s$ and $k_f$ are the solid and fluid thermal conductivities, $R$ is the ratio of the thermal conductivities such that $R > 1$, and $G$ is a geometric factor, which is $\frac{1}{9}$ for spherical particles. It turns out that $F_1$ and $F_2$ are close when $R$ is of the order of 1.

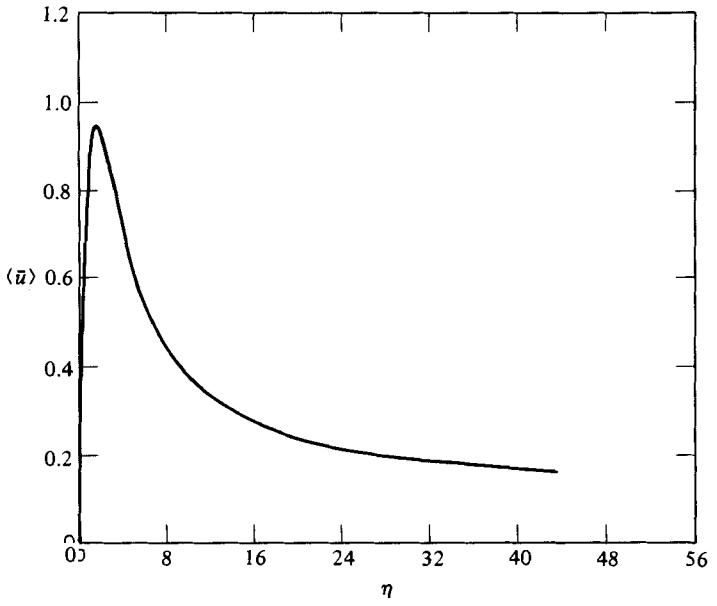


FIGURE 2. The velocity distribution for flow of water through a variable-porosity medium (see table 1).

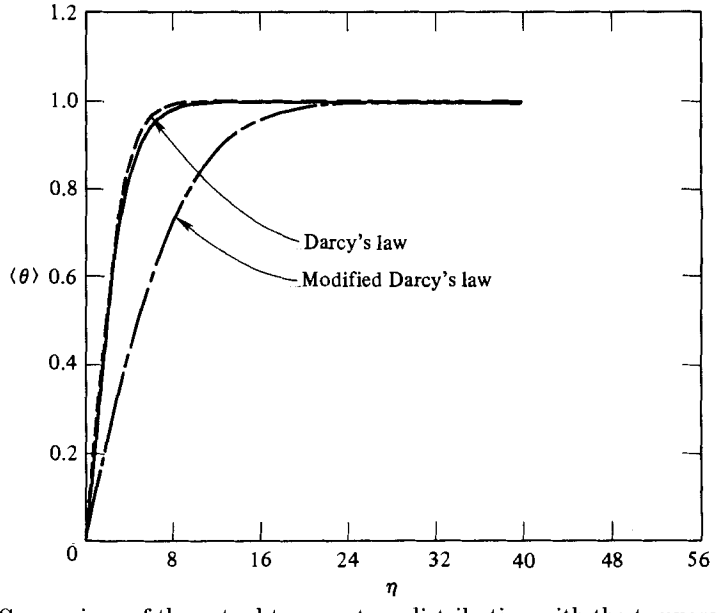


FIGURE 3. Comparison of the actual temperature distribution with the temperature distribution based on Darcy's and the modified Darcy's law.

Therefore the effective thermal conductivity is taken as

$$k_e = \tfrac{1}{2}[F_1(\delta, R, G) + F_2(\delta, R, G)]\,(k_s k_f)^{\frac{1}{2}}. \tag{63}$$

Presented in figures 2–4 are the numerical results for the velocity and temperature profiles for flow of water through a packed bed. The velocity and temperature profiles in figures 2–14 are presented at $\xi = 0.3$. The essential physical information for figures 2–19 is given in table 1. Figure 3 compares the theoretical temperature distribution

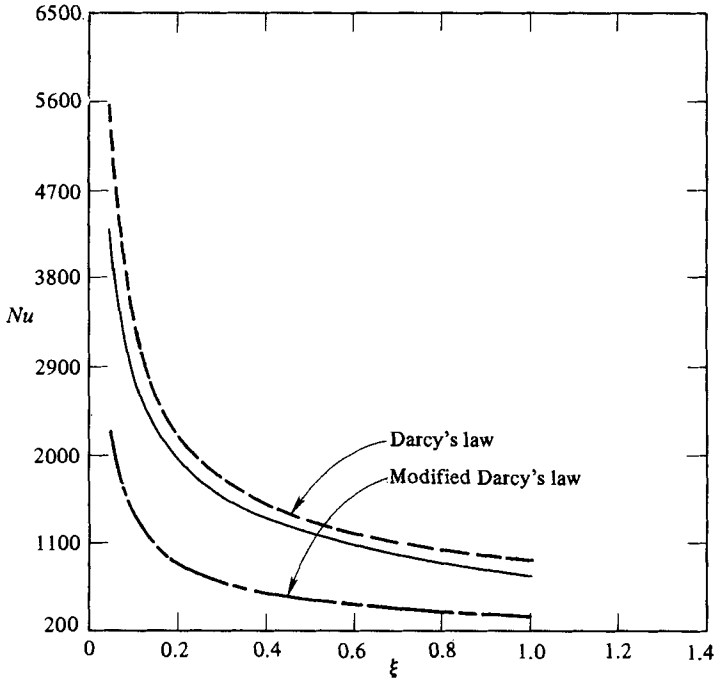


FIGURE 4. The Nusselt-number variations corresponding to the three cases shown in figure 2.

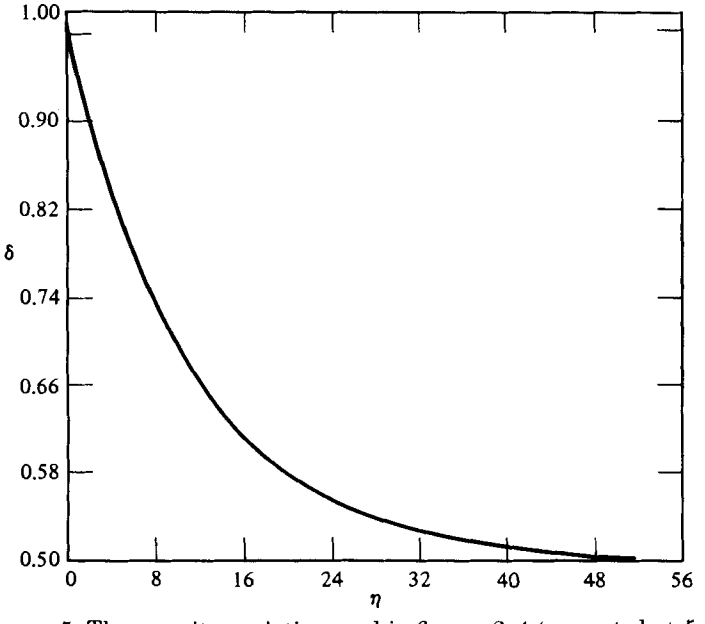


FIGURE 5. The porosity variation used in figures 2–4 (presented at $\xi = 0.3$).

that accounts for all of the effects, with the temperature distribution based on Darcy's law, and also the modified Darcy's law (Forchheimer equation). The Nusselt numbers corresponding to the three cases in figure 3 are shown in figure 4. From figure 4 it is evident that the Nusselt number that accounts for all of the effects lies between the Nusselt number based on Darcy's law and the modified Darcy's law. This behaviour prevailed for most cases for which the effective Prandtl number $Pr_e = \nu/\alpha_e$ was of

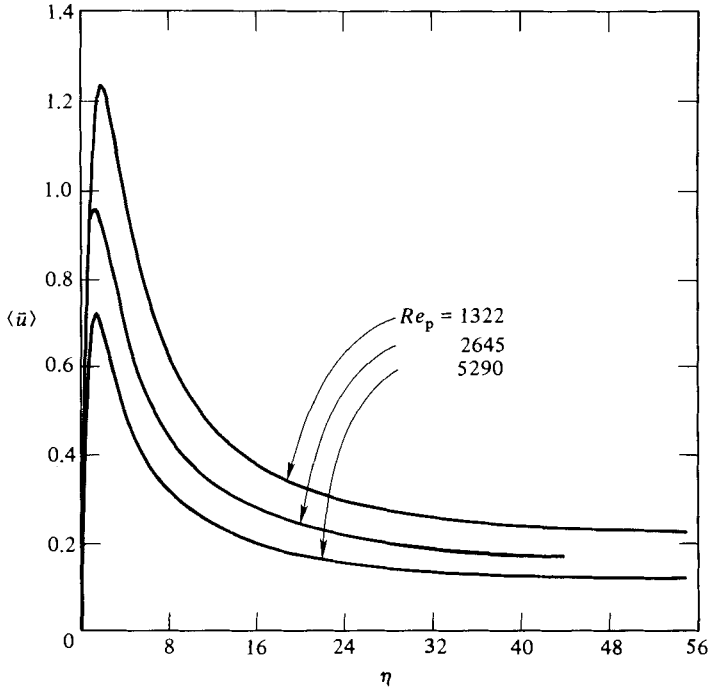


FIGURE 6. The effects of the pressure gradient on the channelling of the velocity distribution (see table 1).

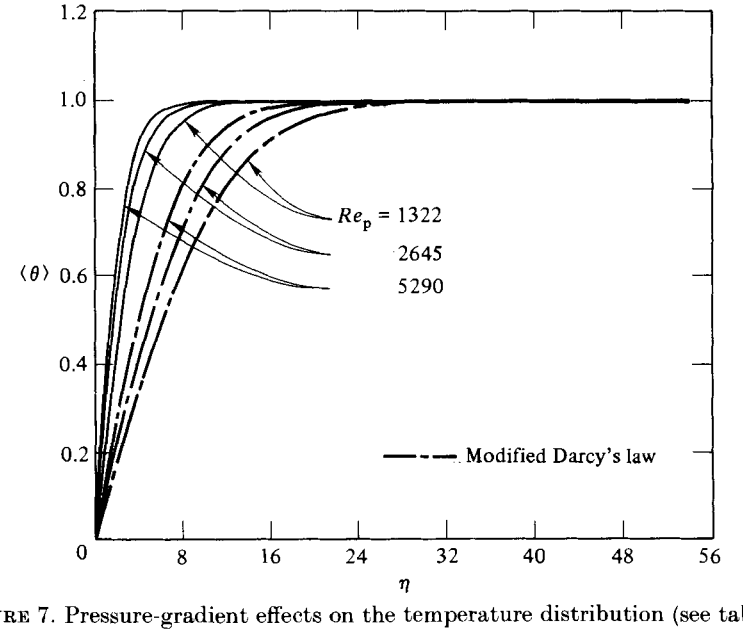


FIGURE 7. Pressure-gradient effects on the temperature distribution (see table 1).

order 1. Therefore it seems plausible to conclude that using Darcy's and the modified Darcy's law is a good estimate for the lower and upper bounds of the theoretical Nusselt number, as long as $Pr_e$ is of order 1. This subject is discussed in more detail later on. The porosity variation used in figures 2–4 is shown in figure 5 for $\xi = 0.3$.

Figures 6–8 show the effects of the pressure gradient on the velocity and

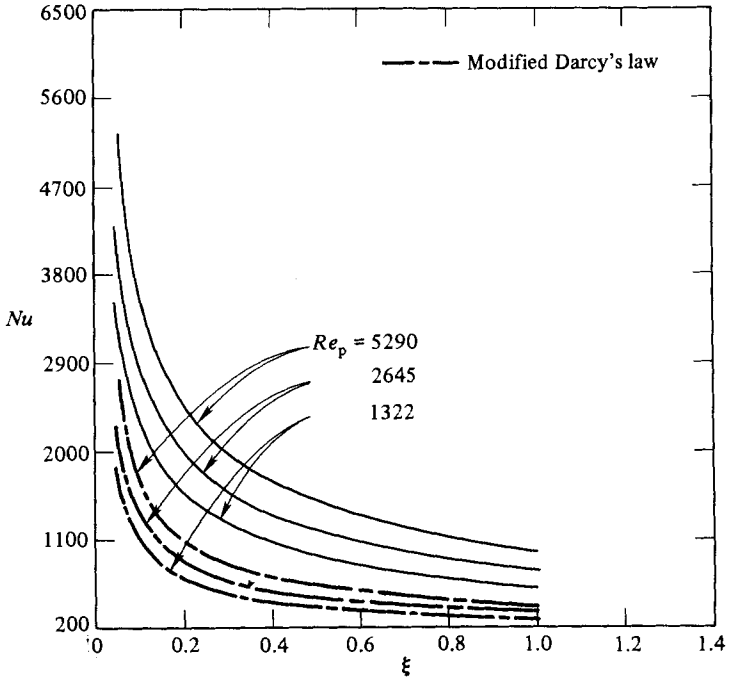


FIGURE 8. Pressure-gradient effects on the Nusselt-number variation (see table 1).

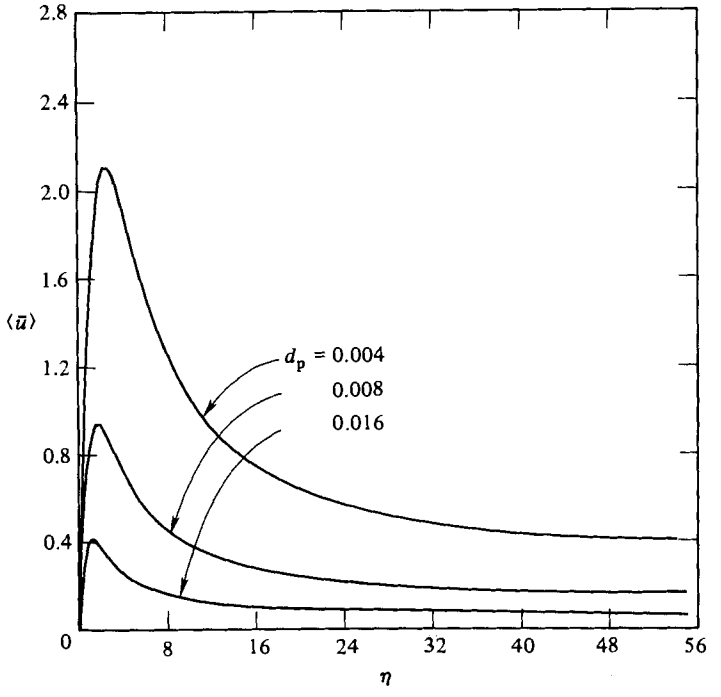


FIGURE 9. The influence of different particle sizes on the channelling of the velocity profile (see table 1).

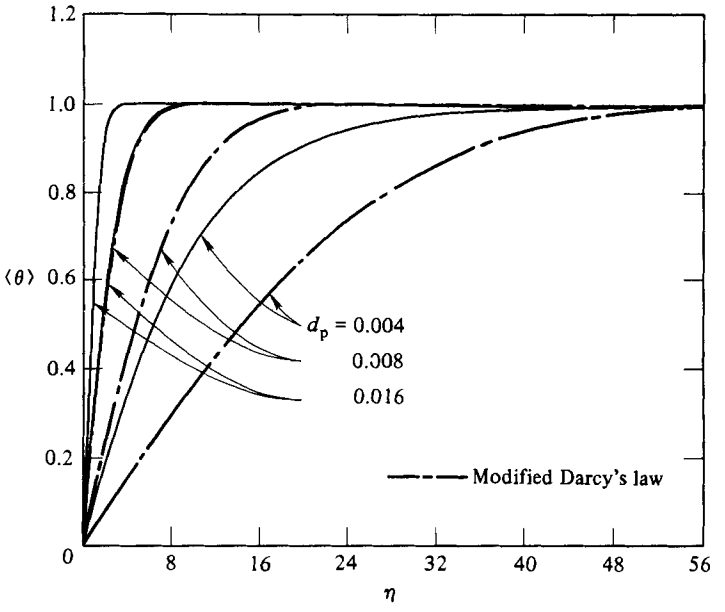


FIGURE 10. Particle-size influence on the temperature distribution for flow through a variable-porsity medium.

temperature distributions. As expected, a higher pressure gradient causes a higher peak velocity. However, it should be noted that the velocities are presented in dimensionless form. To obtain the actual velocity, $\langle \bar{u} \rangle$ should be multiplied by the convective velocity $u_c$. The higher velocities lead to an increase in the convected energy compared with that by conduction, causing a thinner thermal boundary layer for the case that has a higher pressure gradient. This thinner boundary layer creates a larger flux at the boundary leading to the largest values of Nusselt number for the highest pressure gradient. These results are shown in figures 7 and 8. The effects of different particle sizes are shown in figures 9–11. A larger particle size causes a larger permeability, which in turn leads to larger velocities. Therefore smaller particles cause a thicker thermal boundary layer, leading to smaller Nusselt numbers. This is indeed the case, as seen in figures 9–11. The variations in free-stream porosity have a significant effect on the flow field as well as the heat fluxes. These effects are shown in figures 12–14. The larger the free-stream porosity, the smaller the overall frictional damping resistance offered by the porous matrix. This in turn leads to higher velocities for the larger free-stream-porosity case (figure 12). Steeper temperature gradients and larger Nusselt numbers are then created as a result of these higher velocities, as shown in figures 13 and 14. Different values for the constants $b$ and $c$ in (29) generate different porosity variations from the wall. Increasing $b$ causes a higher porosity at the boundary, and increasing $c$ causes the porosity to reach its free-stream value within a shorter distance from the wall. Figure 15 shows that for a larger value of $b$ a larger peak velocity is obtained, irrespective of the variations in $c$. This causes lower Nusselt numbers for the smaller value of $b$. From the same figure it can be seen that, for a fixed value of $b$, decreasing $c$ causes an increase in the peak velocity. This has a direct effect on the temperature field and the Nusselt numbers. At a fixed value of $b$, decreasing $c$ creates steeper temperature gradients and larger Nusselt numbers, as seen in figures 16 and 17.

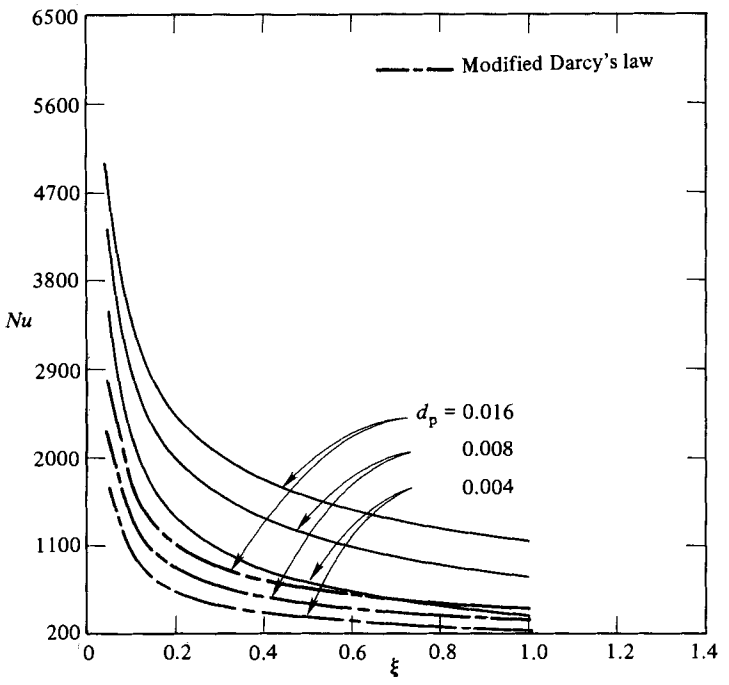


FIGURE 11. The Nusselt-number variation corresponding to particle sizes $d_p = 0.004$ m, 0.008 m and 0.016 m.

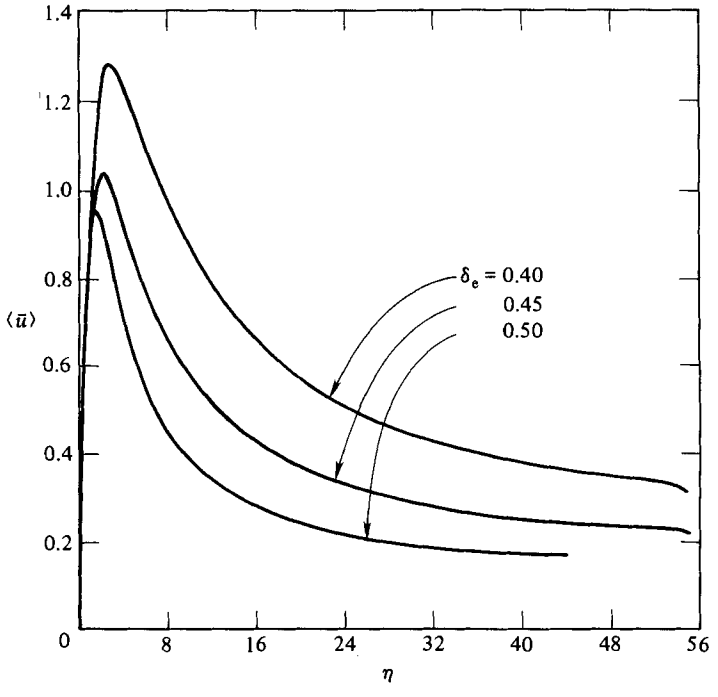


FIGURE 12. Effects of the free-stream porosity on the flow field (see table 1).

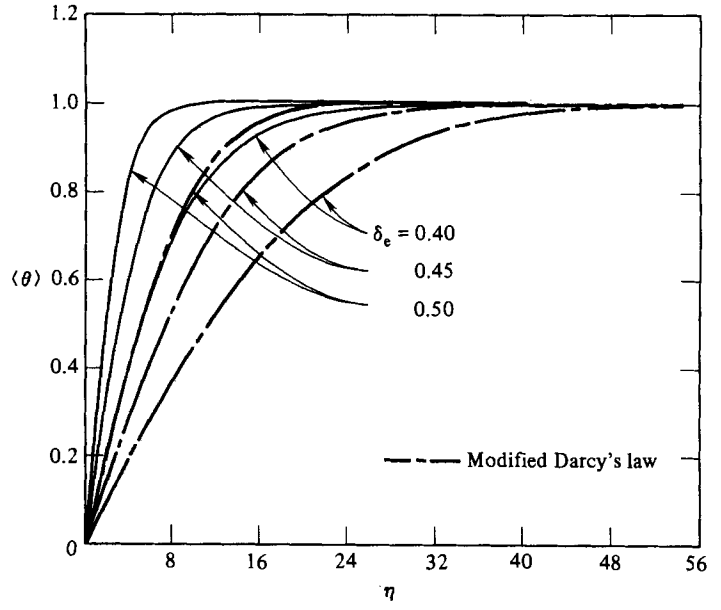


FIGURE 13. Free-stream porosity effects on the temperature field.

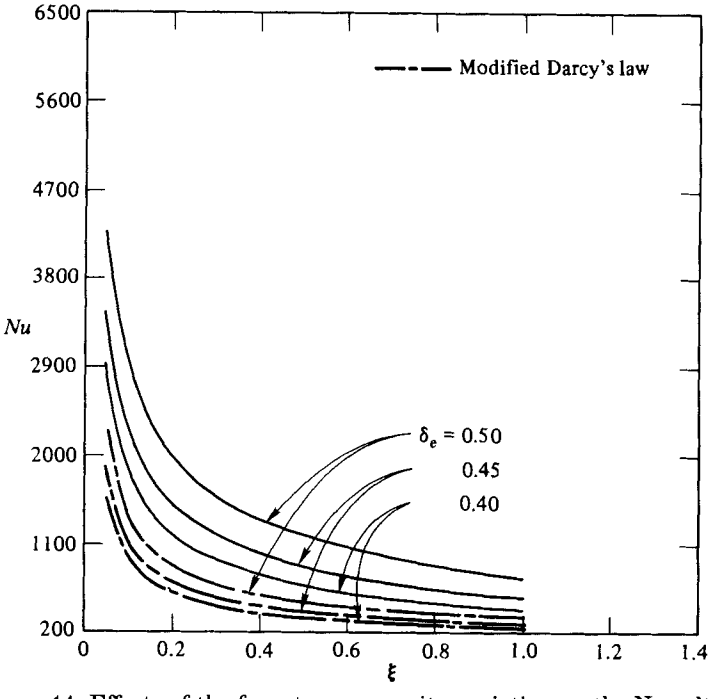


FIGURE 14. Effects of the free-stream porosity variation on the Nusselt number.

The fluid used in all of the above cases was water. To illustrate the significance of different thermophysical properties, the flow of an engine oil though a packed bed is considered next. Aside from the thermophysical properties, all other system parameters are kept the same as those presented in figures 2–5. Figure 18 presents the velocity profiles for different values of the pressure gradient. Higher pressure

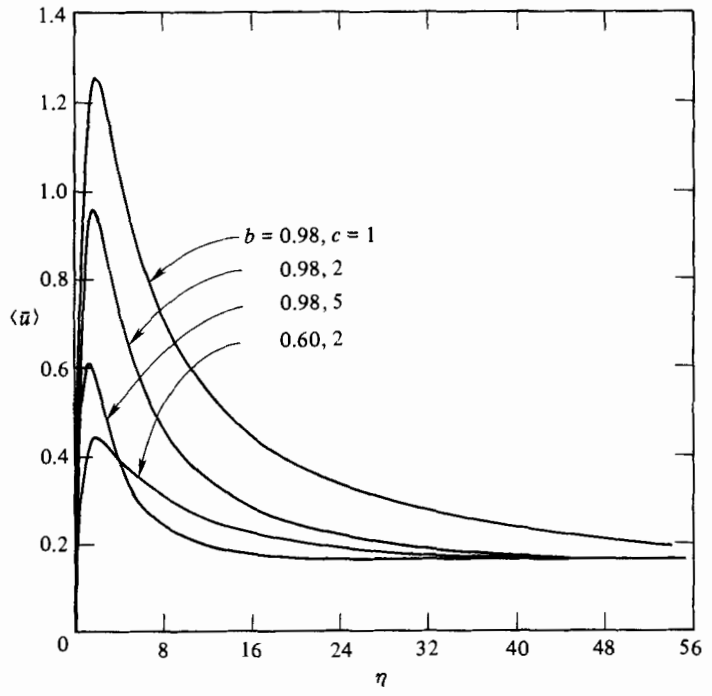


FIGURE 15. Porosity-variation effects on the channelling of the velocity profile.

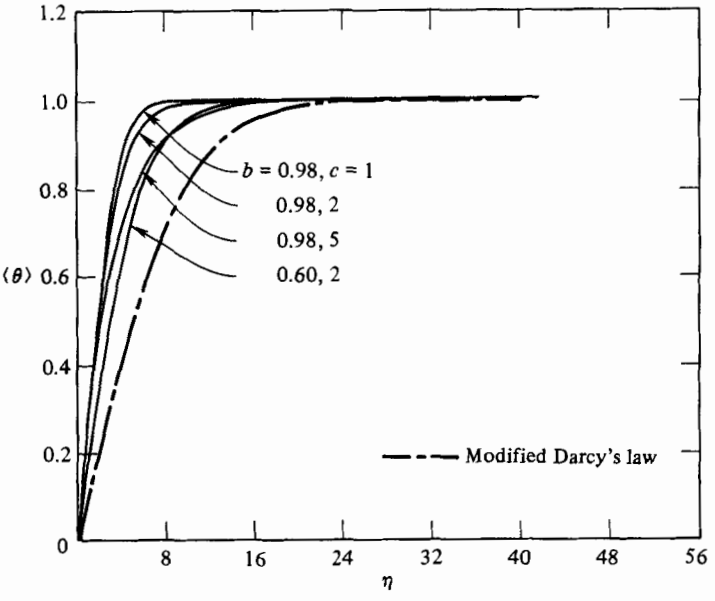


FIGURE 16. Temperature distributions for different porosity variations.

gradients translate into higher values of $Re_p$, which in turn cause higher values of $Q(\eta)$, as seen in (20). The results for the temperature distribution, for $Re_p = 0.189$, are shown in figure 19(*a*). The Nusselt numbers for the case that accounts for all of the inertial forces, variable porosity and the boundary effects, for $Re_p = 0.189$, is presented in figure 19(*b*). Also presented in this figure are the Nusselt numbers based

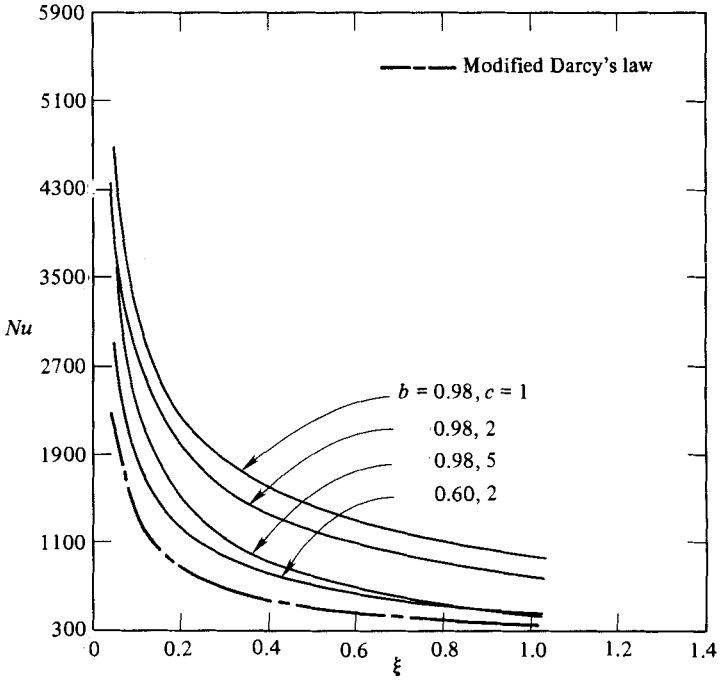


FIGURE 17. Porosity-variation effects on the Nusselt number.

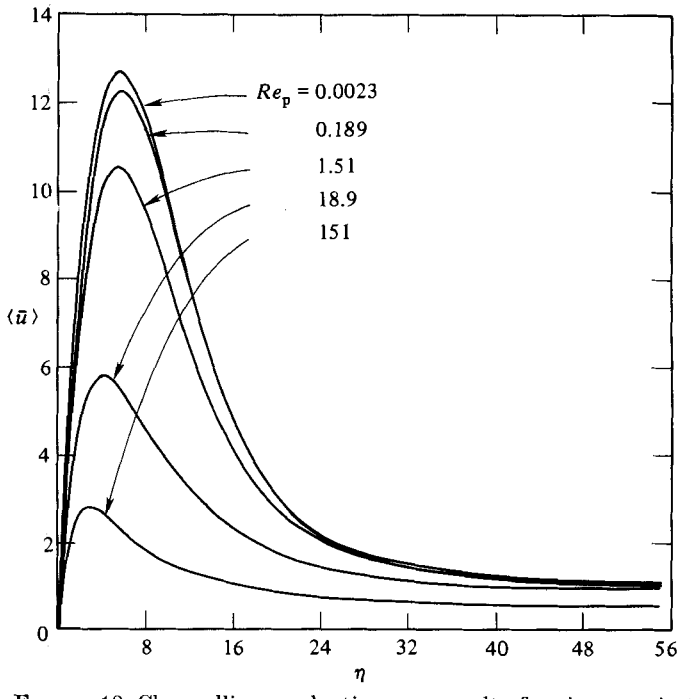


FIGURE 18. Channelling production as a result of an increase in the pressure gradients (see table 1).

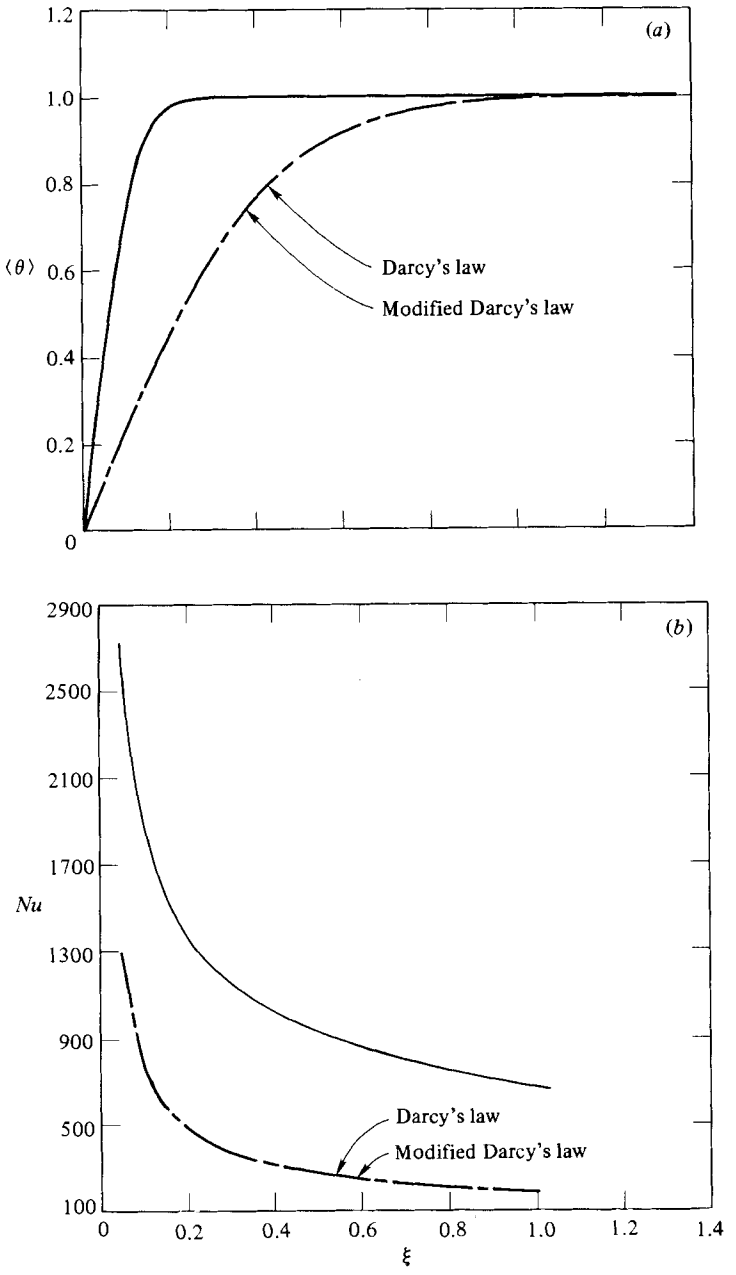


FIGURE 19. The effects of different thermophysical properties on the temperature field and the Nusselt number.

on Darcy's law and the modified Darcy's law. It is seen that for small values of $Re_p$ the inertial effects are negligible and there is almost no difference between the Nusselt number $Nu_D$ based on Darcy's law, and the Nusselt number $Nu_{MD}$ based on the modified Darcy's law. However, the difference between the two Nusselt numbers increases as $Re_p$ is increased. In general, the Nusselt number based on the modified Darcy's law is less than $Nu_D$. This is expected, since the modified Darcy's law provides

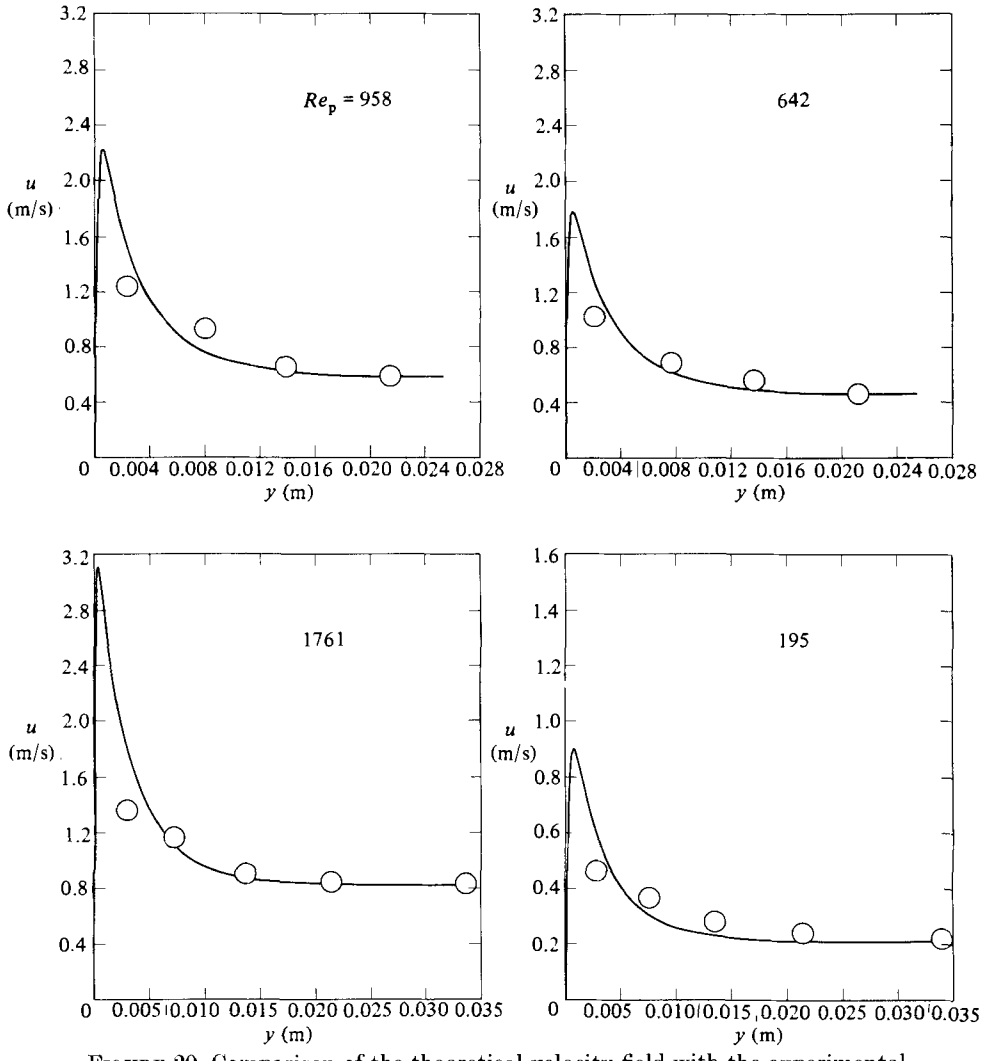


FIGURE 20. Comparison of the theoretical velocity field with the experimental data (open circles) for four different cases.

a lower velocity, which causes less energy to be carried away from the boundary, thus causing a lower Nusselt number. Furthermore, the Nusselt number $Nu$ that accounts for all the effects is usually greater than $Nu_{MD}$. The parameters that affect the ratio $Nu/Nu_{MD}$ are the Prandtl number and the relative magnitude of the peak velocity compared with the Darcy's velocity. For example, for fluids that have an effective Prandtl number of order unity, $Nu$ often lies between the Nusselt number $Nu_D$ based on Darcy's law, and that $Nu_{MD}$ based on the modified Darcy's law. The reason is that for $Pr_e = O(1)$ the momentum boundary layer is of the same order of magnitude as the thermal boundary layer. Therefore, owing to the channelling, the effective convective velocity is greater than the modified Darcy's velocity. This causes more energy to be carried away from the boundary, thus causing $Nu$ to be greater than $Nu_{MD}$.

In the absence of data concentrating on the effects of variable porosity on the heat transfer, the theoretical velocity profile is compared with available experimental

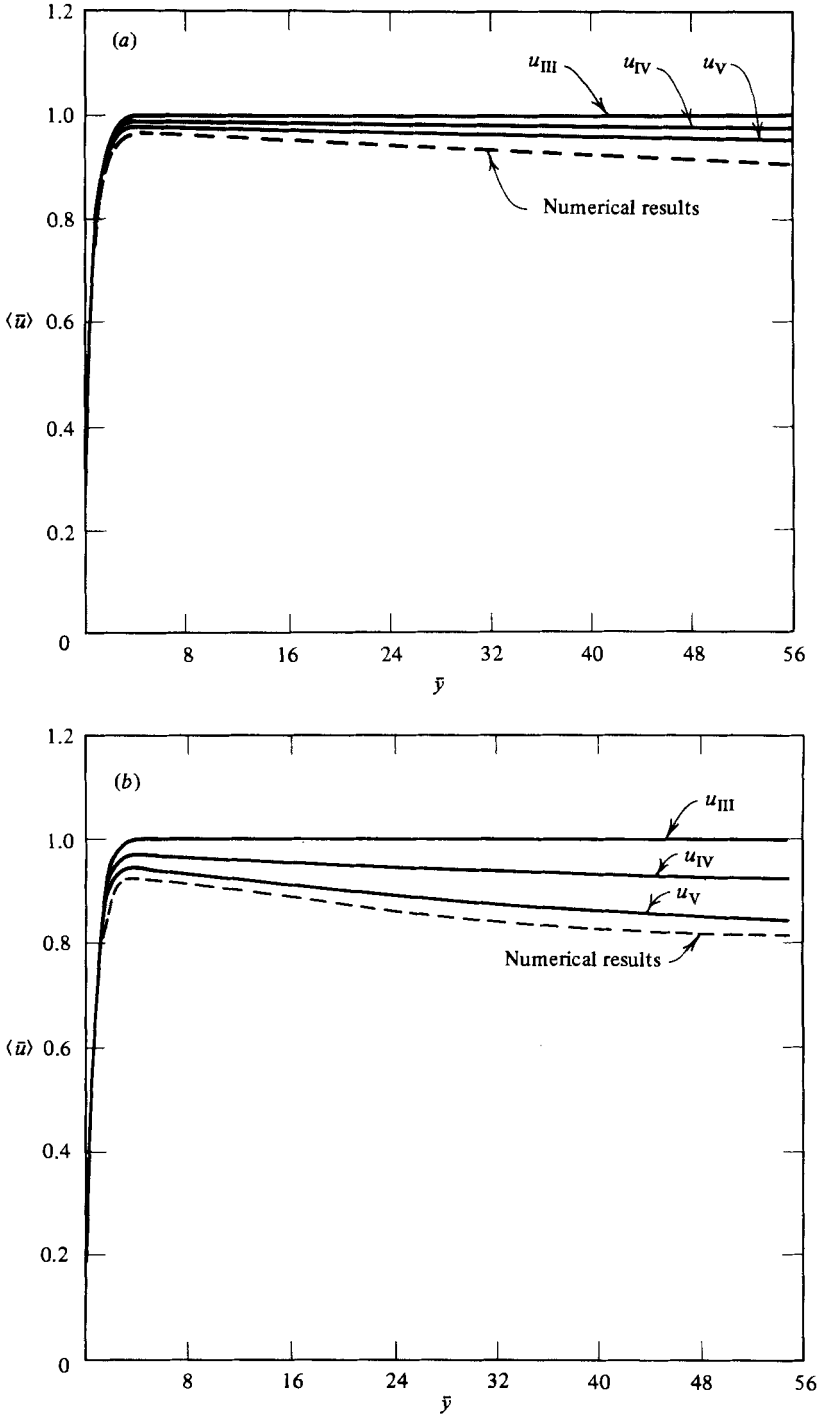


FIGURE 21. Comparison of the numerical and the perturbation solutions for (*a*) $\delta_e = 0.3$, $Re_p = 31$; (*b*) $\delta_e = 0.35$, $Re_p = 51$.

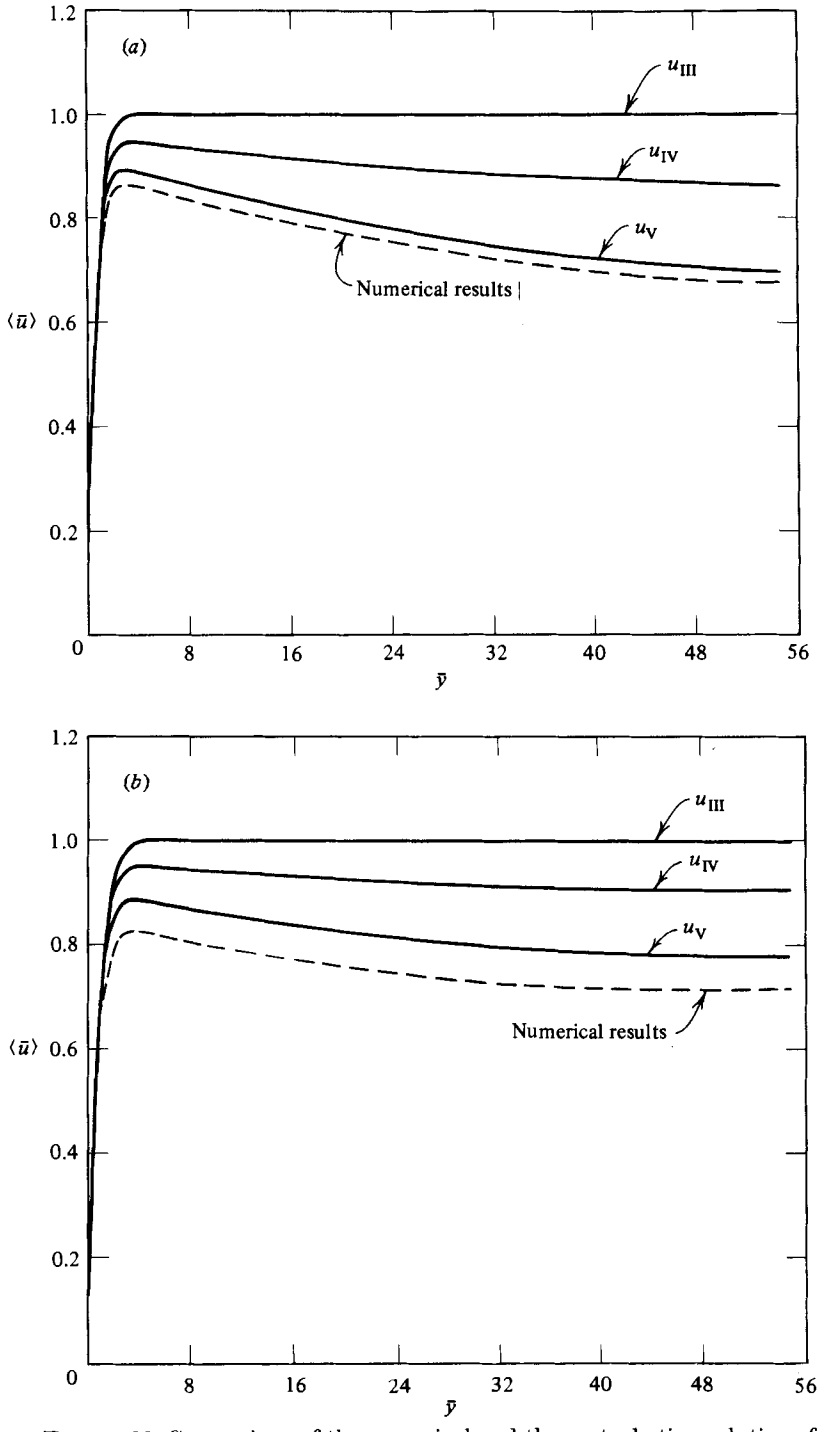


FIGURE 22. Comparison of the numerical and the perturbation solutions for (*a*) $\delta_e = 0.4$, $Re_p = 89$; (*b*) $\delta_e = 0.45$, $Re_p = 60$.

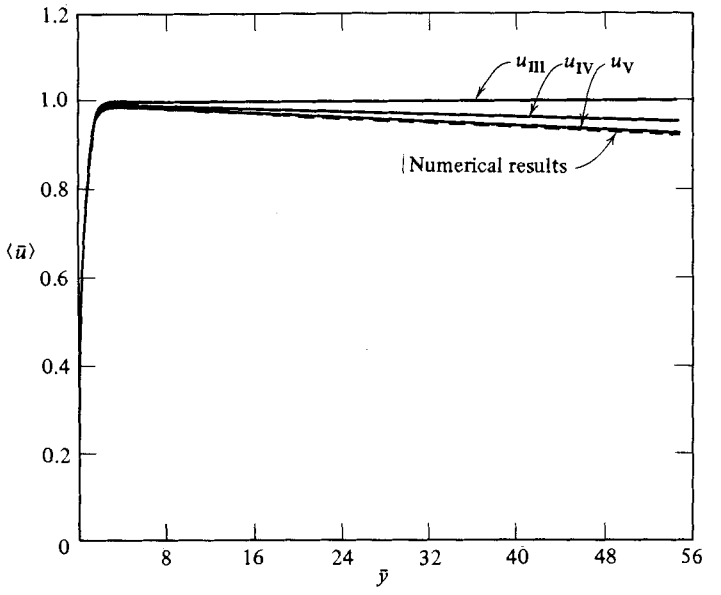


FIGURE 23. Comparison of the numerical and the $u_v$ solutions for $\delta_e = 0.2$, $Re_p = 42$.

data. The comparison is made with the experiments of Schertz & Bischoff (1969). Their experimental set-up included a cylindrical packed bed consisting of stoneware spheres with a diameter of 0.7747 cm. The fluid used in this experiment was air. For this particle diameter and the ratio of bed to particle diameter (13.11) corresponding to their experiment the porosity variation is given by the experiments of Benenati & Brosilow (1962). Using this porosity variation, the theoretical velocity distribution is computed for the same conditions as the experimental data, and is shown in figures 20 for four different runs. The theoretical results were also checked against the experimental results of Schwartz & Smith, and the same kind of agreement was found. As can be seen in figure 20, the agreement between the theory and experimental data is very good. The discrepancies are attributed to the geometry and the small oscillations in porosity, since the oscillations were neglected and a cylindrical geometry was used in the experiments. The numerical results were obtained for a Cartesian system.

In the perturbation solution the inertial forces that are responsible for the channelling effect, for the case where $H_1 = H$, do not appear until the fourth perturbation term. Owing to the packing configuration there is also a physical lower bound for the free-stream porosity $\delta_e$. Therefore there will be a need to carry more terms beyond $\delta_e^5$ for greater accuracy at larger values for $\delta_e$. The shape of the velocity profile as well as the magnitude of the peak velocity and their relation with the porosity variation, the free-stream porosity, the particle diameter and the driving pressure difference becomes very clear after examining the inner and outer solutions given in (46)–(54). For example, the magnitude of the peak velocity and its relation with the porosity variation can be seen by examining the coefficients $Y_{12}$, $R_{16}$ and the outer solutions $u_{4e}$ and $u_{5e}$.

Perturbation solutions for $\delta_e = 0.3$ and $\delta_e = 0.35$ are presented in figure 21 along with the numerical solutions. The numerical results are presented for the same conditions as the perturbation solutions. In this figure $u_{III}$, $u_{IV}$ and $u_V$ refer to the

perturbation solutions that consist respectively of all the terms up to and including the third, the fourth and the fifth. The $u_{III}$ solution contains only the information on the boundary effects. For this reason there is nothing to indicate the formation of a peak velocity. On the other hand, the $u_{IV}$ and $u_V$ solutions clearly indicate the formation of a peak velocity. Furthermore, the $u_V$ solution shows a better peak formation than the $u_{IV}$ solution. In the numerical solution the free-stream conditions were set at the same distance as the perturbation solution. Figure 22 presents the perturbation and the numerical solutions for $\delta_e = 0.40$ and $\delta_e = 0.45$. It can be seen that there is an excellent agreement between the perturbation solution and numerical results, which are presented for the same conditions as the perturbation solution. For values of $\delta_e$ below 0.25 there is very little difference between the $u_V$ solution and the numerical solution. Figure 23 compares the perturbation and the numerical solutions for $\delta_e = 0.2$.

## 6. Conclusions

The purpose of the present study is to show the nature and importance of the channelling effect and its influence on flow and heat transfer through variable-porosity media. This is accomplished by first analysing the general problem, and then applying the formulation to the case of convection in packed beds. The unique dependency of the velocity field on the normal coordinate is established. The qualitative features of the channelling and its production are investigated in depth by the method of matched asymptotic expansions and the numerical solution of the governing equations. The qualitative effects of various controlling parameters on flow and heat transfer are thoroughly investigated and are presented in §5. The variable-porosity effects are shown to be important and significant for most cases. For calculating the heat flux at the boundary, for some cases, Darcy's law provides a better approximation for accounting the variable-porosity effects than the modified Darcy's law. The numerical results are in excellent agreement with the available experimental data.

## Appendix. Perturbation coefficients

The coefficients for (46)–(51) are as follows:

$$\alpha_1 = \frac{-B_3}{4B_2}, \quad \alpha_4 = \frac{-B_3}{4B_2^{\frac{1}{2}}}, \quad Z_1 = \frac{B_3\alpha_4}{8B_2^{\frac{1}{2}}}, \quad Z_2 = \frac{B_3\alpha_4}{4B_2} + \frac{B_4 + B_3\alpha_1}{6B_2^{\frac{1}{2}}},$$

$$Z_3 = \frac{3Z_2}{2B_2^{\frac{1}{2}}}, \quad Z_4 = \frac{Z_3}{B_2^{\frac{1}{2}}}, \quad X_1 = \frac{B_3 Z_1}{12B_2^{\frac{1}{2}}}, \quad X_2 = \left(\frac{5B_3 Z_1}{2B_2^{\frac{1}{2}}} + B_3 Z_2 - \alpha_4 B_4\right) \Big/ 10B_2^{\frac{1}{2}},$$

$$X_3 = \frac{20X_2 - \alpha_1 B_4 - \frac{1}{3}B_5 + B_3\alpha_4 + B_3 Z_3}{8B_2^{\frac{1}{2}}}, \quad X_4 = \frac{12X_3 + 2B_4 + B_3 Z_4 + B_3\alpha_1}{6B_2^{\frac{1}{2}}},$$

$$X_5 = \frac{6X_4 - B_3}{4B_2^{\frac{1}{2}}}, \quad X_6 = \frac{X_5}{B_2^{\frac{1}{2}}}, \quad Y_1 = \frac{B_3 X_1}{16B_2^{\frac{1}{2}}}, \quad Y_2 = \frac{56Y_1 - B_4 Z_1 + B_3 X_2}{14B_2^{\frac{1}{2}}},$$

$$Y_3 = \frac{\frac{1}{3}B_5\alpha_4 + B_3 X_3 + B_3 Z_1 - B_4 Z_2 + 42Y_2}{12B_2^{\frac{1}{2}}},$$

$$Y_4 = \frac{30Y_3 + \frac{1}{12}B_6 - 2B_4\alpha_4 + \frac{1}{3}B_5\alpha_1 + B_3 Z_2 - B_4 Z_3 + B_3 X_4}{10B_2^{\frac{1}{2}}},$$

$$Y_5 = \frac{20Y_4 - B_5 + B_3\alpha_4 - 2B_4\alpha_1 + B_3Z_3 - B_4Z_4 + B_3X_5}{8B_2^{\frac{1}{2}}},$$

$$Y_6 = \frac{12Y_5 + 3B_4 + B_3\alpha_1 + B_3Z_4 + B_3X_6}{6B_2^{\frac{1}{2}}}, \quad Y_7 = \frac{6Y_6 - B_3}{4B_2^{\frac{1}{2}}}, \quad Y_8 = \frac{Y_7 + B_8}{B_2^{\frac{1}{2}}},$$

$$Y_{11} = \frac{B_8}{3B_2}, \quad Y_{12} = \frac{-\psi_1}{(1+b)^3}, R_1 = \frac{B_3Y_1}{20B_2^{\frac{1}{2}}}, \quad R_2 = \frac{90R_1 - B_4X_1 + B_3Y_2}{18B_2^{\frac{1}{2}}},$$

$$R_3 = \frac{72R_2 + \frac{1}{3}B_5Z_1 + B_3X_1 - B_4X_2 + B_3Y_3}{16B_2^{\frac{1}{2}}}$$

$$R_4 = \frac{56R_3 - \frac{1}{12}B_6\alpha_4 - 2B_4Z_1 + \frac{1}{3}B_5Z_2 + B_3X_2 - B_4X_3 + B_3Y_4}{14B_2^{\frac{1}{2}}},$$

$$R_5 = \frac{42R_4 + B_5\alpha_4 - \frac{1}{12}B_6\alpha_1 + B_3Z_1 - 2B_4Z_2 + \frac{1}{3}B_5Z_3 + B_3X_3 - B_4X_4 + B_3Y_5 - \frac{1}{60}B_7}{12B_2^{\frac{1}{2}}},$$

$$R_6 = \frac{30R_5 + \frac{1}{3}B_6 - 3\alpha_4B_4 + B_5\alpha_1 + B_3Z_2 - 2B_4Z_3 + \frac{1}{3}B_5Z_4 + B_3X_4 - B_4X_5 + B_3Y_6}{10B_2^{\frac{1}{2}}},$$

$$R_7 = \frac{20R_6 - 2B_5 + B_3\alpha_4 - 3B_4\alpha_1 + B_3Z_3 - 2B_4Z_4 + B_3X_5 - B_4X_6 + B_3Y_7}{8B_2^{\frac{1}{2}}},$$

$$R_8 = \frac{12R_7 + 4B_4 + B_3\alpha_1 + B_3Z_4 + B_3X_6 + B_3Y_8 - 2B_8\alpha_4}{6B_2^{\frac{1}{2}}},$$

$$R_9 = \frac{6R_8 + B_3A - 2B_8\alpha_1 + 2B_{10} - B_3}{4B_2^{\frac{1}{2}}}, \quad R_{10} = \frac{2R_9 - 2B_9}{2B_2^{\frac{1}{2}}}, \quad R_{12} = \frac{-2B_8\alpha_4}{3B_2},$$

$$R_{13} = \frac{8B_2^{\frac{1}{2}}R_{12} - B_3Y_{11} - 2B_8\alpha_1 + B_{10}}{3B_2}, \quad R_{14} = \frac{4R_{13}B_2^{\frac{1}{2}} - 2R_{12} - B_9}{3B_2},$$

$$R_{15} = \frac{-B_{10} + B_3Y_{12}}{B_2}, \quad R_{16} = \frac{(b-3)\psi_1}{(1+b)^3}, \quad A = -(Y_{11} + Y_{12}), \quad F = -(R_{14} + R_{16}).$$

## REFERENCES


Balakrishnan, A. R. & Pei, D. C. T. 1974 Heat transfer in fixed beds. *Ind. Engng Chem. Proc.* **13**, 441–446.

Benenati, R. F. & Brosilow, C. B. 1962 Void fraction distribution in packed beds. *AIChE J.* **8**, 359–361.

Burns, P. J. & Tien, C. L. 1979 Natural convection in porous media bounded by concentric spheres and horizontal cylinders. *Intl J. Heat Mass Transfer* **22**, 929–939.

Chandrasekhara, B. C. & Vortmeyer, D. 1979 Flow model for velocity distribution in fixed porous beds under isothermal conditions. *Th. Fluid Dyn.* **12**, 105–111.

Cheng, P. & Minkowycz, W. J. 1977 Free convection about a vertical flat plate embedded in a porous medium with application to heat transfer from a dike. *J. Geophys. Res.* **82**, 2040–2044.

Denloye, A. O. O. & Botterill, J. S. M. 1977 Heat transfer in flowing packed beds. *Chem. Engng Sci.* **32**, 461–465.

DeWiest, R. J. M. 1969 *Flow Through Porous Media*. Academic.

Ergun, S. 1952 Fluid flow through packed columns. *Chem. Engng Prog.* **48**, 89–94.

Hughmark, G. A. 1976 Heat transfer in packed beds. *AIChE J.* **22**, 198–199.

Roblee, L. H. S. *et al.* 1958 Radial porosity variation in packed beds. *AIChE J.* **4**, 450–464.

SCHERTZ, W. M. & BISCHOFF, K. B. 1969 Thermal and material transport in non-isothermal packed beds. *AIChE J.* **15**, 597–604.

SCHLUNDER, E. U. 1978 Transport phenomenon in packed bed reactors. *Chem. Reaction Engng Rev.*, pp. 110–161.

SCHWARTZ, C. E. & SMITH, J. M. 1953 Flow distribution in packed beds. *Ind. Engng Chem.* **45**, 1209–1218.

STANEK, V. & SZEKELY, J. 1972 The effect of non-uniform porosity in causing flow maldistributions in isothermal packed beds. *Can. J. Chem. Engng* **50**, 9–14.

TIEN, C. L. & VAFAI, K. 1979 Statistical bounds for the effective thermal conductivity of microsphere and fibrous insulation. *Prog. Astro. Aero.* **65**, 135–148.

VAFAI, K. & TIEN, C. L. 1981 Boundary and inertia effects on flow and heat transfer in porous media. *Intl J. Heat Mass Transfer* **24**, 195–203.

VAFAI, K. & TIEN, C. L. 1982 Boundary and inertia effects on convective mass transfer in porous media. *Intl J. Heat Mass Transfer* **25**, 1183–1190.

WHITAKER, S. 1969 Advances in theory of fluid motion in porous media. *Ind. Engng Chem.* **61**, 14–28.